IEEE Access
Multidisciplinary | Rapid Review | Open Access Journal

Received 9 June 2023, accepted 24 June 2023, date of publication 28 June 2023, date of current version 7 July 2023.

Digital Object Identifier 10.1109/ACCESS.2023.3290217

RESEARCH ARTICLE

HyDNN: A Hybrid Deep Learning Framework Based Multiuser Uplink Channel Estimation and Signal Detection for NOMA-OFDM System

MD HABIBUR RAHMAN[1,2], MOHAMMAD ABRAR SHAKIL SEJAN[1,2], MD ABDUL AZIZ[1,2], YOUNG-HWAN YOU[2,3], AND HYOUNG-KYU SONG[1,2]

[1]Department of Information and Communication Engineering, Sejong University, Seoul 05006, Republic of Korea
[2]Department of Convergence Engineering for Intelligent Drone, Sejong University, Seoul 05006, Republic of Korea
[3]Department of Computer Engineering, Sejong University, Seoul 05006, Republic of Korea

Corresponding author: Hyoung-Kyu Song (songhk@sejong.ac.kr)

This work was supported in part by the Information and Communication Technology (ICT) Research and Development Program of Ministry of Science and Technology/ Information and Communications Technology Promotion (MSIT/IITP) (Research on Core Technology of Autonomous Twins for Metaverse) under Grant IITP-2021-0-01816, and in part by the Basic Science Research Program through the National Research Foundation of Korea (NRF) funded by the Ministry of Education under Grant 2020R1A6A1A03038540.

ABSTRACT Deep learning (DL) techniques can significantly improve successive interference cancellation (SIC) performance for the non-orthogonal multiple access (NOMA) system. The NOMA-orthogonal frequency division multiplexing (OFDM) system is considered in this paper to develop a hybrid deep neural network (HyDNN) model for multiuser uplink channel estimation (CE) and signal detection (SD). The proposed HyDNN uses a combination of a bi-directional long short-term memory (BiLSTM) network and a one-dimensional convolutional neural network (1D-CNN) to optimize errors in the system. The extraction of input signal characteristics from OFDM is carried out using the 1D-CNN model and fed into the time series BiLSTM network to infer the signal at the receiver terminal. The HyDNN model learns through the simulated channel data during offline training. To optimize the loss during learning the model the Adam optimizer is utilized. After successful training, the transmitted symbols in the online deployment are instantly recovered with optimal prediction rates by using the proposed HyDNN model. In comparison to the traditional CE and SD method for the NOMA scheme and other existing DL models, the proposed technique demonstrates satisfactory performance enhancements. In addition, the simulation outcomes show robustness with different training parameters such as minibatch sizes and learning rates.

INDEX TERMS 1D-CNN, BiLSTM, symbol error performance, uplink NOMA, OFDM, multiuser signal detection (SD).

I. INTRODUCTION

The non-orthogonal multiple access (NOMA) scheme has been acknowledged as an effective method for improving spectral efficacy and system performance [1], [2], [3], [4]. The power domain and code domain are two subtypes of NOMA. According to the separation among base stations (BSs) and all users (Us) in the NOMA, the power domain might receive low or high transmission power allocations. By allowing the simultaneous sharing of subcarriers between Us with perfect channel conditions and those with imperfect channel conditions, NOMA maximizes the usage of available bandwidth. As NOMA systems combine signals from multiple Us, inter-user interference must be canceled to decode the signal reliably at the receiver terminal. The state-of-the-art multiuser detection is performed at the detectors of NOMA systems by successive interference cancellation (SIC) with the variations in power domain among Us [5]. Information from various Us is decoded successively in decreasing order of signal power during the SIC operation depending on the channel state information (CSI) [6]. It is challenging to acquire CSI in NOMA due to interference from pilot symbols

The associate editor coordinating the review of this manuscript and approving it for publication was Jie Tang.

used for channel estimation (CE). It may drastically reduce the accuracy of conventional CE procedures, including maximum likelihood (ML), least squares (LS), and minimum mean square errors (MMSE).

To overcome the limitations of the above methods, deep learning (DL) has attracted with great contributions to the field of wireless communications [7] such as CE [8], signal detection (SD) [9], constellation design [10], and modulation recognition [11]. Furthermore, DL applications also have been investigated in 6G system [12], [13] like mmWave [14], reconfigurable reflecting surfaces (RIS) [15] UAV communications [16], respectively. The authors in [17] developed a unique codebook-based architecture for RIS-assisted communications that successfully overcomes the issues of high implementation complexity and significant pilot overhead.

Due to NOMA potential as a future wireless network technology and the aforementioned uses of DL solutions, current research on DL based SD in NOMA-involved systems has gained attention [18], [19], [20]. Using a deep neural network (DNN), a system for estimation of channel parameters of orthogonal frequency-division multiplexing (OFDM) and detecting signals were given in [21]. The authors demonstrated a notable improvement of the performance in terms of symbol-error rate (SER) analysis. In [22], a study on signal detection employing the NOMA technique is presented, which employed DNN based fully-connected model. A similar neural network structure was previously proposed in [21].

By utilizing effective parallel computing techniques, the convolutional neural network (CNN) is able to extract better fundamental properties underlying the channel matrix from the vast amount of data and offers the ability to estimate the channel more precisely with less complexity [23]. This study, utilized 1 dimensional (1D)-CNN model due to the following advantageous reasons over 2D-CNN [24]: (1) A 1D-CNN has much less time complexity than a 2D-CNN under comparable circumstances (same design, network, and hyperparameters), (2) the training hardware demand of 2D-CNN is special configuration (such as cloud computing and GPU) whereas 1D-CNN training can possible quite quick using any CPU structure over a conventional computer, (3) Compact 1D-CNNs are highly suited for real-time and cost-effective implementation because of their low computing requirements, particularly on mobile or handheld gadgets. A CNN technique was proposed in [25] for NOMA system to instantly decode input from numerous Us in a cluster without the usage of conventional signal processing. In [26], the authors proposed 2D-CNN long short-term memory (LSTM) based CE for the NOMA-OFDM system where the proposed technique is applied for the downlink NOMA scenarios and for CNN model flatten layers was used for output vectors. The proposed study achieved a marginal performance than others methods. To solve the imperfect CSI and Us section problems, in [27], authors proposed a CNN-LSTM based downlink NOMA system. The proposed system analyzed the outage probability with a focus on imperfect and perfect CSI.

A feed-forward NN extension known as a recurrent (RNN) may accept input sequences of different lengths. RNNs have the ability to remember the memory of past events and use this data to forecast future values [28]. A form of RNN called LSTM is built with a unique gating mechanism control for accessing memory cells [29]. In [30] authors proposed a three-stage joint channel decomposition and prediction framework based on the two-timescale property and the channel prediction to get the CSI of the time-varying channels in a RIS-assisted system. Additionally, create a new NN structure termed sparse-connected-LSTM to perform channel decomposition and prediction. For an OFDM-NOMA system, LSTM-based CE and SD were also proposed in [20]. The four-layered DL architecture, which consists of one input layer, two LSTM hidden layers, and one output layer, was assessed for bit-error-rate analysis. LSTM based CE and SD are carried out for multiuser NOMA system in [31]. The presented approach evaluated the results based on different cyclic prefixes (CP) and pilot numbers. BiLSTM network is also practical in sequence classification as the data flow in both directions compared with LSTM. Another related study in [32], proposed Volterra-aided CNN and LSTM for mitigating nonlinearity and recovering transmitted signals in visible light communication channel. CNN is used for extracting the implicit feature of channel impairments and LSTM is used for memory sequence prediction. In contrast, our study focused on 1D-CNN with BiLSTM structure for robust feature extraction for radio frequency NOMA communication system. The motivation behind BiLSTM is that it offers additional training capability as the output layers receive information from past (backward) and future (forward) instances simultaneously to provide better accuracy as compared to LSTM [33]. As the flow of information in the BiLSTM network grows, the architecture is able to extract more features from the input data and improve the training capability [34]. According to the experiment results from the study in [35], compared the performance of LSTM and BiLSTM, where BiLSTM has a greater capacity for feature extraction. Our previous study in [36], proposed a CE and SD system based on a BiLSTM network for achieving higher SER output performance. The CE and SD are significantly impacted by the performance in the aforementioned studies. In the NOMA-OFDM based communication systems, the combination of 1D-CNN and BiLSTM may be a potential method to attain high-accuracy performance. Motivated by the above significant advantages of 1D-CNN and BiLSTM and the research gap, in this study, we propose a hybrid (HyDNN) for multiuser uplink CE and SD in NOMA-OFDM systems. The HyDNN consists of a 1D-CNN and a BiLSTM where for assuming a large amount of training data, the 1D-CNN model is added in front of BiLSTM for extraction of channel features thus the combined model improves the learning performance and enhanced the SER. The proposed HyDNN-based receiver solves the SER performance problems of conventional methods more efficiently.

The following is a summary of the study key contributions:

- The HyDNN framework is used in this study to develop the uplink NOMA-OFDM CE and SD system over the Rayleigh fading channel. The NOMA-OFDM problem is solved by the design of the combined 1D-CNN feature extractor and BiLSTM layer. The 1D-CNN model is performed to extract features of the received signal and information to the BiLSTM model is fed for the inference of the original signal at the receiver terminals.
- We segmented the data of the received signals using a 1D-CNN based feature extractor, taking into account inter-carrier interference (ICI) and inter-symbol interference (ISI). The BiLSTM layers are offered for handling the significant ISI generated by the multipath effect and due to the bi-directional structure of BiLSTM, it provides additional training capability for learning the 1D-CNN features with forward and backward directions. Therefore, the output layers receive more feature information for successful signal demodulation and provide better prediction accuracy.
- After offline training, the proposed model can be applied to a multi-user NOMA-OFDM system for online prediction. The concept is validated by employing two users in the simulation system.
- Finally, the effectiveness of HyDNN is performed by calculating SER at different signal-to-noise ratios (SNRs) using the Monte Carlo simulation. The simulation output is compared by learning the model with different minibatch sizes and learning rates for performance analysis. Simulation results have proved that the efficiency of the proposed method is comparable to the conventional NOMA-SIC method outage performance. Moreover, the proposed HyDNN model outperforms the CNN and BiLSTM models, respectively.

The rest of this article is structured as follows: Section II describes the system's data transmission and channel concept, while Section III explains the specifics of the proposed HyDNN model. Section IV presents the simulation findings and complexity. The finding summary is finally presented in Section V.

Notations: The boldface letter in lower case and upper case, respectively, stands for a vector and matrix; The ith element of the vector x is represented by the subscript on the lowercase letter x_i; $(\cdot)^H$, $(\cdot)^{-1}$, $\otimes$ is the Hermitian transpose, inverse, hadamard product, respectively; $\mathbb{E}$ represents the statistical expectation.

II. DATA TRANSMISSION AND SYSTEM CHANNEL MODEL

High spectral efficiency in wireless communications is provided by the multi-carrier modulation technology known as OFDM. Binary inputs are transformed into phase shift keying modulation for mapping to D parallel data streams as part of the modulation process for OFDM. Let $X_a[q]$ represent the qth subcarrier's ath transmit symbol where $a = 0, 1, 2, \ldots, \infty$ and $q = 0, 1, 2, \ldots, Ns - 1$. Transforming signals from the frequency domain to the time domain is done using the inverse fast Fourier transform (IFFT). To avoid interference between symbols, a cyclic prefix (CP) is introduced to the signal. Therefore, the transmitted symbol can be thought of as follows:

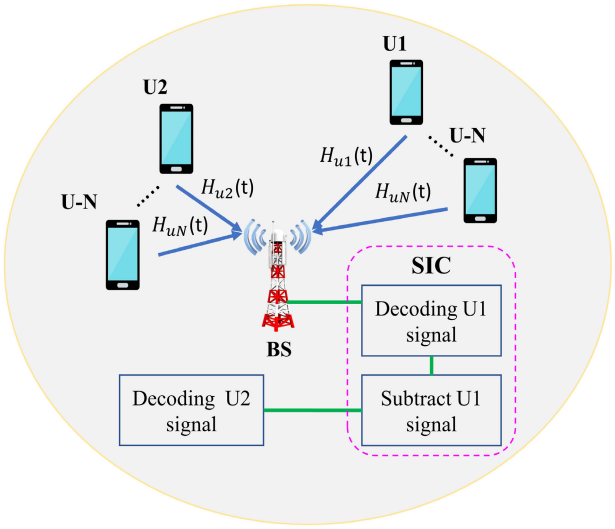

FIGURE 1. The system architecture of NOMA multiuser data transmission from the Us to BS.

$$X_a(n) = \sum_{q=0}^{Ns-1} X_a[q] e^{j(2\pi qn/Ns)} \quad n = 0,\ 1,\ 2 \ldots,\ N_s - 1 \tag{1}$$

where N_s is the FFT length.

In this paper, an uplink NOMA system is assumed. The multiuser uplink NOMA system, which comprises of a BS and two Us (U_u, $u = 1, 2, \ldots .N$), is depicted in Fig. 1. In this system, it is assumed that all the nodes are constructed with individual antenna and both Us transmit data at the same time with identical frequency resources. The BS receives a superposition of data symbols from two Us with channel noise from the transmitter, which employs a traditional NOMA-OFDM scheme. The power allocation is done with the assumption that the transmitter and receiver are aware of CSI. Moreover, for the estimation and detection of the channel, a pilot symbol is inserted into the system. On the other hand, the multiuser side employs the HyDNN approach for flexible CE and SD.

For the NOMA system, the superposition of data symbols for the N Us can be expressed as follows [22]:

$$y = \sum_{u=1}^{N} \sqrt{P_u} X_u, \tag{2}$$

where P_u and X_u are defined as the power allocation and the transmitted baseband symbol for U_u.

If the OFDM system is formatted with K-subcarriers and has N Us, the following is an expression for the received

signal on subcarriers k:

$$y(k) = \sum_{u=1}^{N} \sqrt{P_u}(k) h_u(k) X_u(k), \tag{3}$$

where the FFT of the impulse response of a multipath channel and the received frequency-domain signal respectively, are $h_u(k)$ and $y(k)$. $X_u(k)$ is a representation of U_u's transmitted symbol.

For the k subcarriers, at the receiver, the white additive Gaussian noise (AWGN) $W(k)$ is denoted by the symbol $\mathcal{CN}(0, \sigma^2)$. Following the addition of the AWGN, the received signal may be written as follows:

$$y(k) = \sum_{u=1}^{N} \sqrt{P_u}(k) h_u(k) X_u(k) + \boldsymbol{W}(k). \tag{4}$$

The power allocation P_u for the u Us with k subcarriers is rewritten as $P_u(k)$. However, the total power P_w is allotted to each of the k subcarriers in the OFDM. The following is an expression for the U_u's power allocation coefficient:

$$\delta_u(k) = \frac{\boldsymbol{P}_u(k)}{\boldsymbol{P}_w}. \tag{5}$$

The following formulation can be used to express the constraint of equation (5) [26]:

$$\sum_{u=1}^{N} \delta_u(k) = 1. \tag{6}$$

Therefore, the impulse response of a multipath channel FFT $\boldsymbol{h}_u(k)$ for the U_u is stated as follows [37]:

$$H_u(t) = \sum_{m=1}^{M} \upsilon_{u,m} \eta(t - \tau_{u,m}), \tag{7}$$

where $\upsilon_{u,m}$ and $\tau_{u,m}$, respectively, stand in for the complex channel gain and associated time delay for the Us' mth multipath parameters. The channel is represented by Rayleigh fading in the proposed work, where the total number of determined pathways M is taken into account to be 20.

The signal is estimated and detected by the CSI using conventional SIC techniques like LS and MMSE [38]. Additionally, ML detectors are utilized to predict signals since U_u signals are given greater power [39]. For the uplink CE of LS and MMSE, pilot data transmission is employed. So the conventional LS CE of (4) can be expressed as follows [38]:

$$\hat{\boldsymbol{h}}_{LS} = \frac{\boldsymbol{y_p}}{\boldsymbol{X_p}}, \tag{8}$$

where $\boldsymbol{X_p}$ is the transmitted pilot sequences $\boldsymbol{P} = \boldsymbol{p_1}, \boldsymbol{p_2}, \ldots \boldsymbol{p_N}$ and $\boldsymbol{y_p}$ is the received pilot data for estimation of channel parameters. In addition for estimation of MMSE, the correction coefficient $\mathbf{R}_{hh_{LS}}$ is calculated. The estimation of MMSE can be formulated as follows [38]:

$$\begin{aligned} \hat{h}_{\text{MMSEu}} &= \mathbf{R}_{hh_{LS}} \mathbf{R}^{-1}_{h_{LS}h_{LS}} \hat{h_{LS}} \\ &= \mathbf{R}_{hh} \left(\mathbf{R}_{hh} + \sigma_s^2 (\mathbf{X_p} \mathbf{X_p}^H)^{-1} \right)^{-1} \hat{h}_{\text{LSu}}, \end{aligned} \tag{9}$$

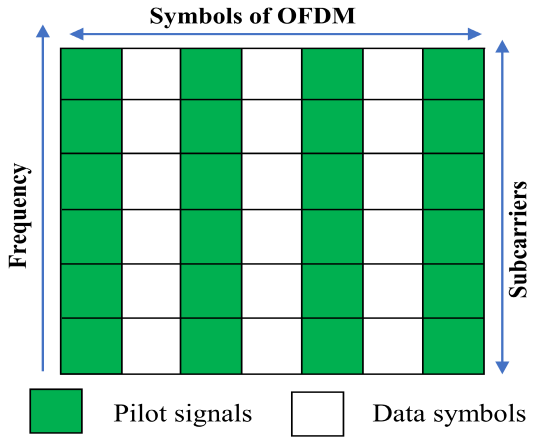

FIGURE 2. Block-type pilot signal insertion structure.

where the signal is transmitted from the uth transmit antenna, $\hat{h}_{\text{MMSEu}}$ is the MMSE estimated for the channel, $\hat{h}_{LSu}$ is the LS estimation of the uth transmit antenna, and AWGN channel noise variance is σ_{s^2}.

These covariance matrices can be expressed as follows:

$$\mathbf{R}_{hh} = \mathbb{E}\{\mathbf{h}\mathbf{h}^H\}, \tag{10}$$

$$\mathbf{R}_{hh_{LS}} = \mathbb{E}\{\mathbf{h}\hat{\mathbf{h}}_{\mathbf{LS}}{}^H\}, \tag{11}$$

$$\mathbf{R}_{h_{LS}h_{LS}} = \mathbb{E}\{\hat{\mathbf{h}}_{\mathbf{LS}}\hat{\mathbf{h}}_{\mathbf{LS}}{}^H\}, \tag{12}$$

where (10) is defined as channel autocorrelation matrix of frequency-domain with expectation operator $\mathbb{E}$, (11) is the cross-correlation among the actual channel and predicted channel which is estimated via LS estimator with the size of FFT $\times$ pilot, $\mathbf{P}$. MMSE estimator can increase the accuracy of CE because it considers the impact of noise and it needs the prior information on channel characteristics which enhances the computational complexity compared to LS. However, each U transmits a pilot symbol $\mathbf{P}$, to the BS, and this pilot is used for the CE. The second U signal, $y_2'(k)$, can be calculated after the first U signal has been estimated which can be formulated as follows:

$$y_2{}'(k) = y(k) - \sqrt{P_1}\hat{h}(k)\hat{X}_1(k). \tag{13}$$

A. INSERTION OF PILOT DATA TO THE OFDM

The pilot signal is known as symbols which are inserted on OFDM subcarriers to get the information for the channel response. The operation of CE and SD is done based on these pilot responses. Block-type pilot insertion strategy that is most widely utilized and adopted [40]. Fig. 2 shows the design of a block-type insertion of the pilot, where the green and white squares indicate the value of the pilot signal and data signal, respectively.

The pilot and data symbols of block-type are individually inserted between each pair of subsequent OFDM signals. Either just pilot or only data symbols are contained in the single OFDM signal. Additionally, as shown by the obtained

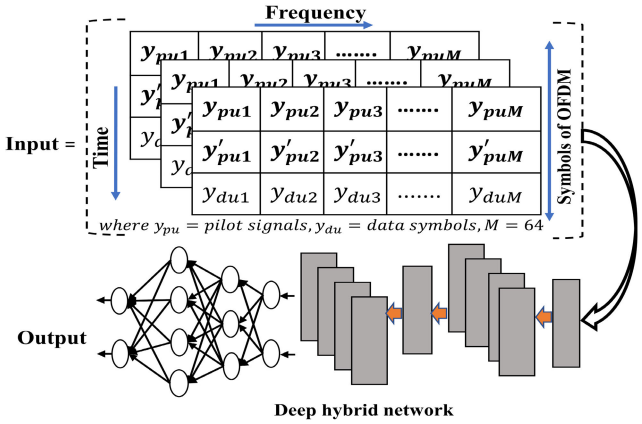

FIGURE 3. Training input dataset of the proposed model.

pilot and data responses, the signal is detected at the conclusion of two successive OFDM symbols [41].

III. PROPOSED HyDNN MODEL

In this paper, the proposed HyDNN network is formed by combining 1D-CNN and BiLSTM models. The 1D-CNN model output is cascaded with the BiLSTM model (i.e, the input of the BiLSTM model is the model output of 1D-CNN). The receiver objective is to retrieve the sent symbols for multiuser usage according to the presented model at the BS. The proposed network is trained with the channel characteristics using the OFDM simulation data which are generated with a certain channel profile.

A. DATASET PREPARATION

To ensure optimal CSI and SD performance, data generation and model construction of the DL network are very crucial points. In this subsection, the dataset generation procedure is discussed.

In this paper, the subcarrier length is 64 of the OFDM system for the generation of the training dataset is considered. The data is transmitted from an OFDM packet and 1 OFDM packet contains 3 OFDM symbols such as 1 data stream $(y_{du1}, y_{du2}, y_{du3}, \ldots..y_{duM})$ and 2 pilot data symbols $(y_{pu1}, y_{pu2}, y_{pu3}, \ldots..y_{puM})$, $(y'_{pu1}, y'_{pu2}, y'_{pu3}, \ldots..y'_{puM})$, respectively as shown in Fig. 3. In the multiuser case, the first 2 OFDM symbols are generated by each U as 2 pilot sequence, and the third OFDM symbol occupies the transmitted 1 data symbol. The previous section II-A provides a description of the specifics of pilot data insertion. Considered is the quadrature phase shift-keying (QPSK) modulation, which uses 2 bits per subcarrier for each symbol. In order to create an OFDM packet with fixed pilot sequences, QPSK random data symbols are used in the training data preparation. The Rayleigh fading channel is used to send the OFDM packets to the receiving end. The BS on the receiving end receives the combined OFDM packet from all Us together with extra AWGN noise in order to decode the OFDM packets.

Algorithm 1 Training Data Generation Process

1: Initialize data: **T** is total packet, N is number of OFDM subcarriers, N_{sc} is pilot subcarrier, M_{cp} is the CP length, **EdB** is SNR value
2: **for** each EdB value in **EdB**
3: **for** n = 1: **T**, generate training data for each class, N_l.
4: Random generation of Rayleigh channel coefficients and AWGN W noise.
5: Generate fixed pilot symbols and insert them to compose the pilot-OFDM symbol.
6: Randomly generate $Nlog_2M_u$, for Us $u = 1, 2, \ldots N$ bits and map them X_u by M_u-ary modulation. Then obtain y symbols according to Eq. (2).
7: According to Eq. (4), calculate the received signal y transmission through Rayleigh channel coefficients in step 4, and based on the y, obtain the $(Y_{du}^{R_e}, Y_{du}^{I_m}, Y_{pu}^{R_e}, Y_{pu}^{I_m})$
8: **end for**
9: **end for**
10: Outputs $(Y_{du}^{R_e}, Y_{du}^{I_m}, Y_{pu}^{R_e}, Y_{pu}^{I_m})$
11: Save the generated data

By constructing a feature vector called **F**, the received OFDM packet is saved as a sample for the training data set. The real, R_e, and imaginary, I_m values of each symbol in the OFDM packet are combined to form the feature vector **F**. The amount of the training sample is equal to the product of the total number of data packets (T) and the total number of labels (N_l). The proposed HyDNN network may be taught to recover data on any subcarrier k by employing the corresponding $L(k)$ in the training process. Multiuser transmission symbols are assigned to a single integer value label for classification. There are a total of 2^4 combinations or labels available in the system for Us transmitting QPSK symbols. However, for $N_l = 16$, the entire label may be written as $L(k) = 1, 2, 3, 4 \ldots..N_l$. 1 OFDM packet has three OFDM symbols, 2 active Us, and a total input size of 384 as the 64 subcarriers are taken into account. Data samples totaling $50000 \times N_l = 800000$ are created for training, using 50000 data packets. The whole generated data sample is divided into two portions, such as train and validation data size, in order to create the model as effectively as possible. The size of the training data sample is (4/5), or 640000, while the validation data sample is (1/5), or 160000. The process of training data generation is summarized in the **Algorithm 1**.

B. 1D CONVOLUTIONAL NEURAL NETWORK DESCRIPTION

The proposed 1D-CNN network is depicted on the left side in Fig. 4. 1D-CNN architecture model for extraction of signal features is used. The input layer is fed into an OFDM data symbol with an input dimension equal to the quantity of features in the input. Convolutional 1D, ReLU, and normalizing layers are the following layers. Every neuron in the convolutional layer gets input characteristics from a rectangular area

of the previous layer, resulting in a rectangular grid of neurons in this layer. In order to condense the output of the convolutional layer into a single vector, a global average pooling 1D layer is utilized last. The goal of the 1D-CNN network is to local feature extraction and through the sharing parameters reduce the number of weights. Thus, the calculation of the overall network is effectively reduced by 1D-CNN.

C. BiLSTM NETWORK DESCRIPTION

On the right side of Fig. 4 the BiLSTM model framework is illustrated. The motivation for proposing the BiLSTM network is as follows. The unidirectional LSTM networks perform sequences in the past, without considering the future. This is due to the fact that unidirectional LSTM only retains information from earlier time steps since it only receives input from the past [42]. On the other hand, the BiLSTM is comprised of the forward (one from past to future) and backward (one from future to past) directions of the unidirectional LSTM. The input flows both ways, allowing it to utilize both sides of the information, offering additional training feature extractions and improving the prediction performance. Fig. 5(a) and (b) display a schematic representation of the internal cell architecture of the unidirectional LSTM and BiLSTM, respectively. BiLSTM hidden, fully connected, softmax function and classification layers are among the 4 layers that make up the proposed BiLSTM model. There are 100 hidden units used to implement the BiLSTM hidden layer. The fully connected layer is executed with a 16 number of classes. The outputs for the end layer are obtained by using the softmax function. The classification layer is used in the final layer to convert the output to a vector probability.

D. MATHEMATICAL OPERATION OF CNN-BiLSTM

Input Layer: The input for 1D-CNN is comprised of the sequence of real and imaginary values with corresponding labels. Let the input sequence features matrix of F=[${S_1}^{R_e}$, ${S_1}^{I_m}$, ${S_2}^{R_e}$, ${S_2}^{I_m}$, ..., ${S_N}^{R_e}$, ${S_N}^{I_m}$], which is composed of two numerical values together and their label classes. The ith output of the sequence matrix is S_i, so that S_0=F. Each sequence contained 384 real, R_e, and imaginary, I_m values and which represent the label, N_l. The dimension of 384×1 is assumed to represent the size of the input features in the input layer. The input layer of the CNN is fed the two numerical values of sequence features with its label from the generated dataset, where there are the same number of features in the input data as the input size.

Convolutional 1D Layer ($i = 1$): The convolutional layer function is fed to the sequence inputs and extracts local features from it. A group of learnable filters makes up the parameters for the convolutional layer ($k \times s$, where k denotes the kernel size and s denotes the dimension of the input data). A total of 32 filters in 3×3 different sizes are used in the convolutional layer for the feature extraction. Accordingly, the output feature matrix S_i can be expressed as follows:

$$S_i = f(S_{i-1} \otimes w_i + b_i), \tag{14}$$

where w_i is denotes weight for ith layers and b_i is denotes the bias for ith layers. The ReLU (rectified linear unit) activation function is used in the next layers which is a non-linear or piece-wise linear function. The ReLU function output is directly input if it is positive, else, the output will be 0. The mathematical formulation of the ReLU function is as follows: $f(x) = max(0, x)$.

1-D Global Average Pooling Layer ($i = 2$): To minimize the information dimension and the likelihood of network overfitting, the pooling layer is primarily utilized to compress the features that the convolutional layer has extracted. A 1-D global average pooling method is used in this study where the main role of this layer is the reduction of sequence features computational time from prior hidden layers. The maximum of the prior features matrix is produced by the pooling layer. As a result, the output feature matrix S_i can be written as follows:

$$S_i = f_p(S_{i-1}) \tag{15}$$

where the pooling function is f_p. The dimension of S_2 is $m/z \times n$ which is obtained from the pooling layer, where z stands in for the current layer's scale value in the pooling layer, the input data time steps are denoted by m, and the quantity of filters is defined by n.

BiLSTM Layer ($i = 3$): The input gate, output gate, and forget gate make up a BiLSTM cell. Each time slot sequence into and out of the cell is controlled by these three gates. As the BiLSTM network flows the information in both directions, more training features from both directions are recorded for mapping Us transmitting in the successive time slot. The mathematical formulation of BiLSTM is as follows. For input signal S_2 at the current time step t, the calculation of BiLSTM layers in both directional flows can be expressed as follows:

$$\overrightarrow{h_{3_f}} = \sigma(W_{3_f} S_{2_t} + W_{3_f} h_{3_{t-1}} + b_{3_f}), \tag{16}$$

$$\overleftarrow{h_{3_r}} = \sigma(W_{3_r} S_{2_t} + W_{3_r} h_{3_{t+1}} + b_{3_r}), \tag{17}$$

where σ is the activation function, the time steps of forward and backward represent $t-1$ and $t+1$, the hidden state of previous and next are $h_{3_{t-1}}$ and $h_{3_{t+1}}$, respectively, the weights and learnable bias of both directions is W_{3_f} and W_{3_r} and b_{3_f} and b_{3_r}, respectively, and finally, the forward and backward direction LSTM network outputs are $\overrightarrow{h_{3_f}}$ and $\overleftarrow{h_{3_r}}$ respectively. Therefore, the output S_3 of BiLSTM can be formulated as follows:

$$\begin{aligned} S_3 &= \sigma(W_{S_3} \overrightarrow{h_{3_f}} \oplus W_{S_3} \overleftarrow{h_{3_r}} + b_{S_3}) \\ &= \sigma(W_{S_3} \tilde{h}_{3_t} + b_{S_3}), \end{aligned} \tag{18}$$

where the output weights of the BiLSTM network are W_{S_3}, the learnable parameter of BiLSTM output bias is b_{S_3}, the concentration of the hidden state at both directions of BiLSTM is $\tilde{h}_{3_t}$.

Fully Connected Layer ($i = 4$): The fully connected layer is very important and its work is to classify whereas a method of activation, the softmax is chosen. Particularly, the

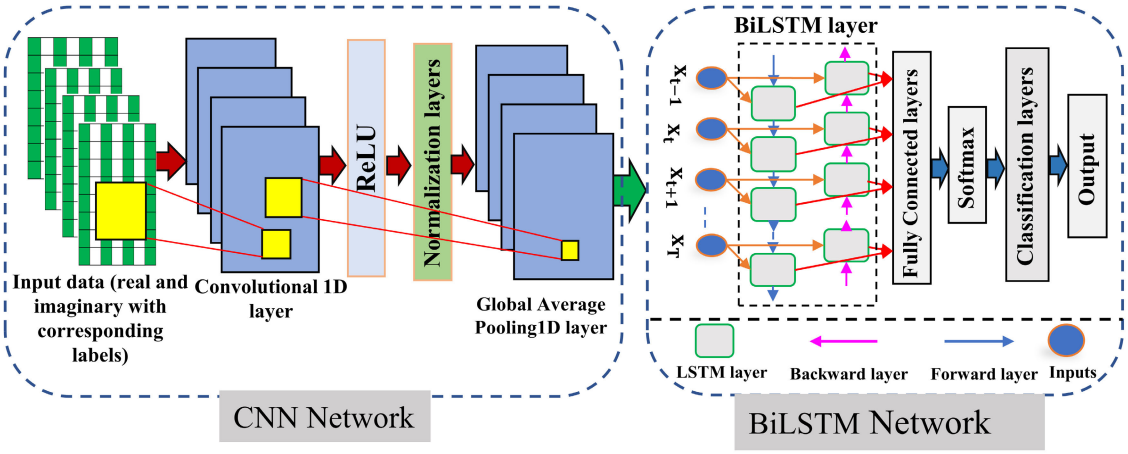

FIGURE 4. The proposed HyDNN model architecture connection of its different layers: the 1D-CNN network structure is on the (left side) and the BiLSTM network structure is on the (right side).

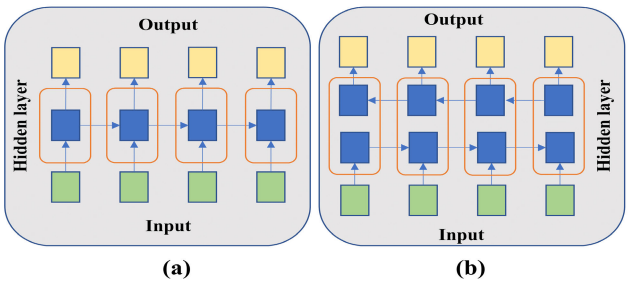

FIGURE 5. Internal cell structure of one layer: (a) LSTM; (b) BiLSTM.

final classification is performed by the fully connected layer. Here, the model estimates the probability that each sample presently belongs to each class and then derives a features expression (Y_{pred}) that can be stated as follows:

$$Y_{pred}(i) = f(L = l_i | S_3; (W, b)) \tag{19}$$

where the features from the BiLSTM layer are S_3 and the softmax activation function is $f(\cdot)$. l_i represents the calculation output of the ith classes of the input data, and the weight and bias value are represented by W and b, respectively.

The cross-entropy operation calculates the cross-entropy loss for single-label and multi-label classification tasks between network predictions and target values. When working with models of output probabilities, cross-entropy is typically the best option. Additionally, $L2$ regularization can be seen as a successful compromise between locating small weights and lowering the cost function [43]. Cross-entropy and $L2$ regularization are therefore used to avoid overfitting. Reducing the computation of loss is the goal of training the model that is formulated as follows:

$$Loss(W, b) = -\sum_{i=1}^{n_s}\sum_{t=1}^{c}(Y^{(t)}(i) * \log(Y^{(t)}_{pred}(i)) + \frac{\lambda}{2}\sum_{i=1}^{n_s} W_i^2 \tag{20}$$

where $(Y^{(t)}(i)$ stands for the prospect of the known goal, $(Y^{(t)}_{pred}(i))$ is the probability that the ith sample belongs to the tth class, the sample numbers is n_s, the class size is c, and finally, λ is used to define the regularization coefficient of $L2$. The Adam optimization technique is applied to reduce the loss [44].

E. HyDNN MODEL TRAINING AND TESTING PROCESS

Based on the design and data generation of the proposed DL network architecture, the training procedure is done in the offline. The offline training of the proposed HyDNN model is shown in the upper part of Fig. 6. The generated dataset is split into two portions: training and validation for learning of the model. According to Fig. 6 in the upper part, the proposed HyDNN model is loaded as sequential inputs of the training and validation data to the input layer of the 1D CNN model and the corresponding labels as supervised information. The dimension of sequence input of CNN is 384×1.

The input layer is fed into these sequential data with label values together. The vector of input features is then learned by the convolutional 1D layer with the learnable parameters (weights=$3 \times 384 \times 32$ and basis=1×32). Then the learnable CNN is fed into BiLSTM input. The total hidden units of BiLSTM are summed up forward and backward which is $100 + 100 = 200$, where the weights of input dimension are 800×32, weights of recurrent dimension are 800×100, and bias is 800×1. The fully connected layer is then classified, and the softmax is used as an activation function. The output dimension of the model is 16×1. Thus, the operation of the HyDNN model is done and it is called for training as HyDNN described in **Algorithm 2**.

Table 1 shows the training and optimized parameters for training setting the HyDNN. The training and validation performance is done with a total of 100 epochs to learn the model. Furthermore, it has been found that the learning rate performance of the proposed model is extremely robust

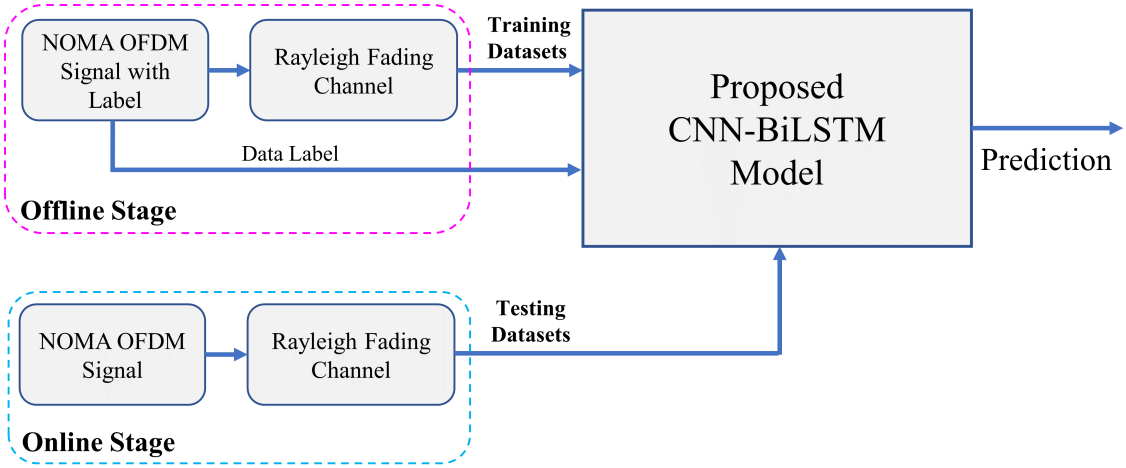

FIGURE 6. Training and testing procedure of the proposed HyDNN model: the training mechanism in the offline stage (upper part); the testing mechanism in the online stage (bottom part).

TABLE 1. The simulation parameters of proposed HyDNN model.

Parameters	Value
Subcarriers of OFDM	64
Number of Pilots	64
Multipath numbers	20
Channel Noise	AWGN
Number of cyclic prefixes (CP)	20
fading channel	Rayleigh channel
U numbers	2
Modulation scheme	QPSK
Numbers of total packets	50,000
Numbers of layers in model	9
Total Epochs	100
Fully connected layer	16
Hidden state units	100
Learning rate (LR)	0.01, 0.001
Size of minibatch	500, 1000, 2000, 5000, 8000
Optimizer	Adam

in relation to the iteration and epoch values. The testing method begins in the online stage once the proposed HyDNN model has undergone consecutive training. With the training settings of 500 for the minibatch size and 0.01 for the learning rate, the validation accuracy is attained at a rate of 99.93. The lower part of Fig. 6 shows the online testing process that the testing datasets test the trained HyDNN model where the channel characteristics are tested as input to match the true and predicted values for optimal prediction calculation.

In the online deployment process, for evaluating the system performance, the trained model is loaded and initialized with the parameters of testing data of the NOMA-OFDM signal over the Rayleigh fading channel. Then the SER simulation results of the proposed model are obtained in different SNR values. The details of the situation evaluations are represented in section **IV**. The training and testing procedure for the proposed network overview is provided on **Algorithm 2**.

Algorithm 2 HyDNN Training and Testing Process

Training procedure:
1: Load the data symbols: assuming $(Y_{du}^{R_e}, Y_{du}^{I_m}, Y_{pu}^{R_e}, Y_{pu}^{I_m})$
2: split the data samples into a training and validation set at a ratio of 80% and 20%.
3: Passing processed data to build the model and configure the layers.
4: Setting the model parameters like learning rate, maximum epochs, and minibatch size.
5: Loss function calculation by (20).
6: Using the Adam optimization technique, find the best solution while updating the parameters and computing the correction parameter.
7: Save the model.
8: Output: HyDNN model.
Testing procedure:
9: Load the trained HyDNN model.
10: Initialize the all parameters.
11: **for** e: 1 to Iteration **do**:
12: **for** n: 1 to SNR **do**:
13: Data symbols transmit through channel matrix.
14: Received data symbols.
15: Generate test label classes from received data symbols
16: Match the label classes with the trained model to classify.
17: SER performance with different SNR.
18: **end for**
19: **end for**
20: Output: SER results.

IV. SIMULATION PERFORMANCE EVALUATION

In this paper, the simulation work is conducted on the Windows 10 Pro operating system. The program is performed with MATLAB. The DL network formation is performed by interconnecting DL layers which are provided in the DL

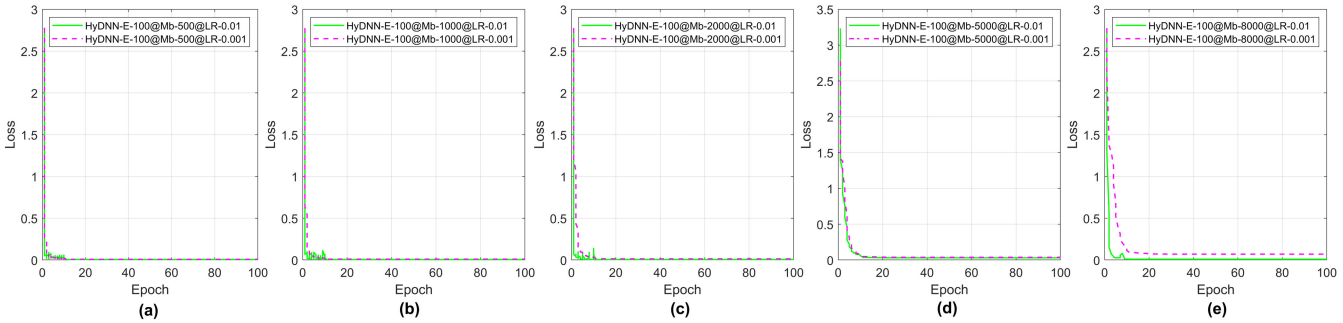

FIGURE 7. Different hyperparameters tuning effect of HyDNN and CNN models with; (a) Epoch=100, minibatch (Mb) size=500 and learning rate=0.01 and 0.001, (b) Epoch=100, minibatch (Mb) size=1000 and learning rate=0.01 and 0.001, (c) Epoch=100, minibatch (Mb) size=2000 and learning rate=0.01 and 0.001,(d) Epoch=100, minibatch (Mb) size=5000 and learning rate=0.01 and 0.001, (e) Epoch=100, minibatch (Mb) size=8000 and learning rate=0.01 and 0.001.

Toolbox^{TM}. The DL Toolbox^{TM} also provides Us with the creation of DL models and monitors the training process. An NVIDIA graphic card is utilized to enhance training performance. The simulation outcomes are done using the various simulation settings listed in Table 1 for the proposed HyDNN-based multiuser CE and SD. The training data information in the previous section III-A was explained. For generating the training dataset, the SNR value is considered at 30 dB in the offline stage. Evaluation of the simulation results with an SNR range of [0: 2: 30] dB is done in order to test the trained model in the online stage. To infer the model and obtain the optimal results, 3000 packets for testing the trained model are used. For evaluating the SER performance of the proposed HyDNN network, Monte Carlo simulations are provided. 64 pilots in each transmitted package, and a CP size of 20 during training and testing are utilized to compare the proposed model with traditional MMSE, LS, and ML methods and CNN and BiLSTM models.

To illustrate the system performance, the proposed network with conventional SIC approaches such as MMSE, LS, ML, as well CNN, and BiLSTM models are used. In this proposed system, two different Us are considered. As a result of the ICI and ISI not being totally eliminated, the MMSE-SIC findings are not ideal for the distorted practical settings [22].

A. PERFORMANCE EVALUATION

To get the optimal prediction performance, the tuning of hyperparameters is very important at the time of learning the model. To get the best-learned model, the proposed model is trained with a variety of hyperparameters. Figure 7(a) and (b) shows the hyperparameters comparison of HyDNN and CNN models with loss function versus different epochs value of 100, minibatch=500, 1000 and learning rates=0.01 and 0.001, respectively. In addition, Figure 7(c), (d), and (e) shows the hyperparameters comparison of HyDNN and CNN models with loss function versus different epochs value of 100, minibatch=2000, 5000, 8000 and learning rates=0.01 and 0.001, respectively. The loss function of these results is taken under SNR 30 dB. It is seen from

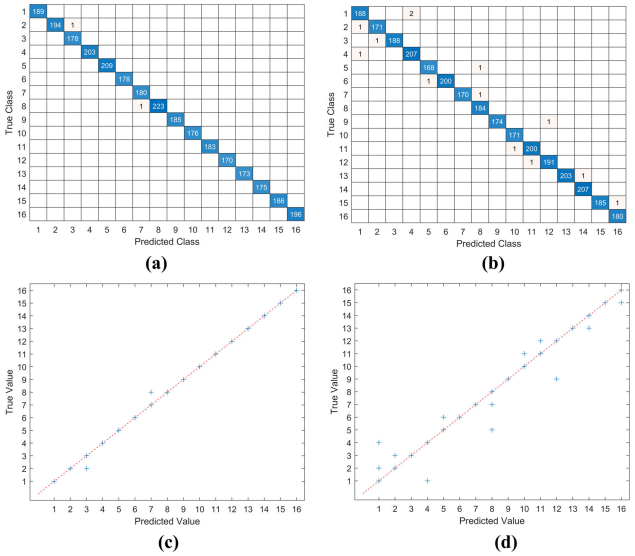

FIGURE 8. (a), (b): Confusion matrix results for multi class symbol classification according to true class and predicted class at minibatch 500 with a learning rate of 0.01 and 0.001. (c), (d): Correlation of true and predicted results for multi classes symbol classification according to true class and predicted class at minibatch 500 with a learning rate of 0.01 and 0.001.

the above graph, by increasing the learning rate and minibatch size, the performance is achieved better. With the decrease in learning rate and increased minibatch, the convergence time is decreased. However, the loss value is increased which caused the degradation of CE estimation performance. For getting better CE estimation and avoiding over-fitting risk, it is kept learning rates=0.01 and 0.001 and minibatch=500.

The simulation results are conducted by comparison of different traditional signal estimation and detection schemes. The results of a simulation using a confusion matrix show how robust the model symbol categorization is during testing. Fig. 8 illustrates the confusion matrix and correlation for symbol categorization based on the number of labels. In Fig. 8(a) and (b), the confusion matrix results for the mini-

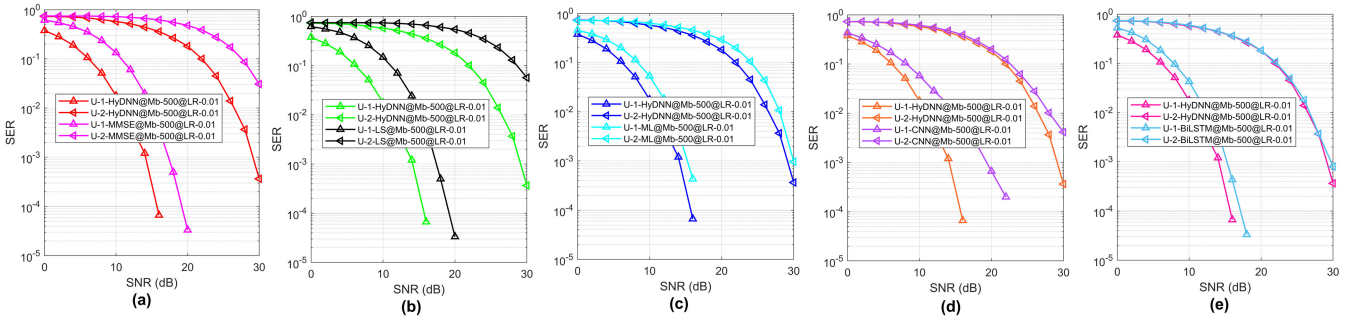

FIGURE 9. SER achievement of the proposed HyDNN model with two Us for NOMA-OFDM system; (a), (b), (c) and (d) are SNR versus SER achievement for the proposed model and traditional (MMSE, LS, ML) methods, CNN model at minibatch (Mb) size 500, and learning rate 0.01 during training.

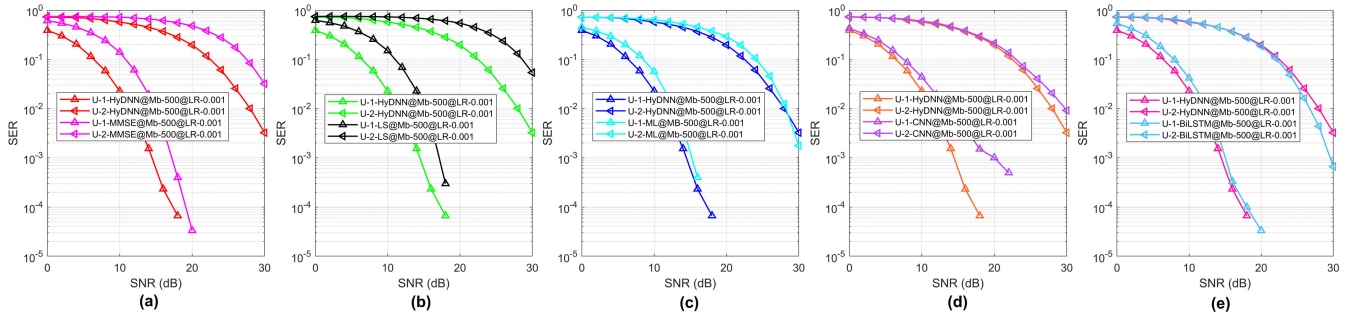

FIGURE 10. SER achievement of the proposed HyDNN model with two Us for NOMA-OFDM system; (a), (b), and (c) (d) are SNR versus SER achievement for the proposed model and traditional (MMSE, LS, ML) methods, CNN model at minibatch (Mb) size 500, and learning rate 0.001 during training.

batch size 500 with the learning rates of 0.01 and 0.001 are shown, respectively. In contrast, correlation results of true and predicted values for minibatch size 500 with the learning rates of 0.01 and 0.001, are shown in Fig. 8(c) and (d). The proposed HyDNN model has a very high symbol decoding and classification rate, which grounds true class and predicted class matching with the exception of a few small missing classes.

In Fig. 9(a), (b), (c), (d), and (e) the SER performances of the HyDNN model are compared with the conventional (MMSE, LS)-SIC, ML method, CNN and BiLSTM model for U-1 and U-2 are shown respectively. With a minibatch size of 500 and a learning rate of 0.01, the proposed model is compared against existing approaches. The proposed model is compared to the ML approach with the ideal scenario of perfect CSI circumstances. According to Fig. 9(a) and (b), the proposed model achieved 16 dB SNR whereas the MMSE and LS achieved 20 dB SNR. In addition, in Fig. 9(c), the ML also achieved less performance than the HyDNN model. The performance of the proposed HYDNN is also evaluated in comparison to that of the CNN and BiLTSM models to determine its efficacy. It is observed that the CNN model achieved 22 dB SNR and the proposed model gained 6 dB SNR more than the CNN model. It is also seen that the proposed HyDNN model outperforms the BiLSTM model as well.

On the other hand, Fig. 10(a), (b), (c), (d), and (e) depict the SER performance of the proposed model with MMSE, LS, ML, CNN, and BiLSTM at the minibatch size of 500 and a learning rate of 0.001 for both Us. Additionally, it is stated that the proposed model consistently outperforms CNN and BiLSTM models as well as conventional approaches in terms of SER performance. However, Fig. 10(c) shows that the SER accuracy of the ML methods is a little higher than the proposed network at the end of the curve with high SNR for U-2. In Fig. 10(c), the ML performance is higher after the SNR of 28 dB for U-2. This small degradation happens due to the low learning rates of the model and the ideal case of the ML technique. With the lower learning rate and same minibatch size, the performance of the proposed model is achieved 18 dB SNR which is 2 dB degradation than the learning rate of 0.01. However, though the performance of the proposed model is a little degraded with less learning rate, still the SER performance is higher than all other methods as well as the CNN and BiLSTM models. From the above discussion, it can be stated that the proposed HyDNN-based receivers can handle the ICI and the ISI using 1D-CNN and BiLSTM based networks very effectively. It is also observed that information about the interconnections among subcarriers by the convolution for the input sequence of the proposed model is also possible to extract. With the exception of a little deterioration, the proposed detection network outperforms all of the approaches in the overall cases as shown in Fig. 11(a) and (b).

In order to examine the learning capacity of the proposed HyDNN model, the simulation outcomes are also done in

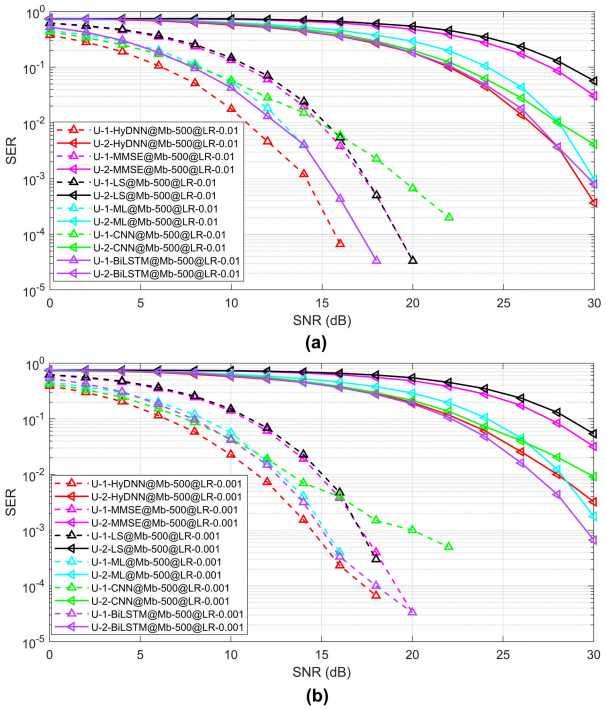

FIGURE 11. Overview of SER performance of the proposed HyDNN model with two Us for NOMA-OFDM system; (a) with learning rate 0.01, (b) with learning rate 0.001.

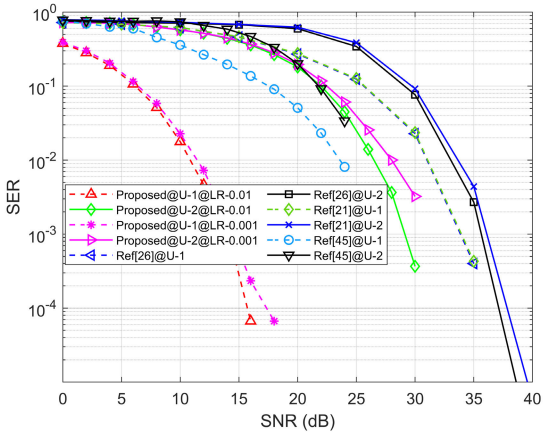

FIGURE 12. Comparison results of the proposed system in terms of SER achievement and different SNR values.

TABLE 2. Testing performance evaluation of the proposed HyDNN.

Mini-batch (Mb)	Epoch (E)	Learning Rate (LR)	Testing Acc. (%)
500	100	0.01	99.93
		0.001	99.56
1000	100	0.01	99.86
		0.001	99.46
2000	100	0.01	99.83
		0.001	99.30
5000	100	0.01	99.73
		0.001	98.60
8000	100	0.01	99.60
		0.001	96.60

terms of testing precision utilizing SNR $(0-30)$ dB values of the final Monte Carlo simulations. Table 2 provides an illustration of the testing accuracy findings using various SNR settings. The proposed model is trained with the mini-batch size 500, 1000, 2000, 5000, and 8000 is considered by the learning rate of 0.01 and 0.001. The evaluation of the proposed HyDNN model performance for the SER using SNR values demonstrated that testing accuracy varies very little with varied minibatch and learning rates. However, the average variation of accuracy is not much different with different parameter settings. The testing accuracy for different SNR values is 99.93 and 99.56 percent for 500 minibatch and learning rates of 0.01 and 0.001, respectively. The achieved accuracy with simulation parameters is showing best among all of the outcomes which shows the robustness of the inference capacity of the proposed model.

The simulation results of various schemes are shown in Fig. 12, where the curves show the effectiveness for channel estimation and signal detection of the proposed HyDNN model, DNN in [21], DNN in [45] and CNN-LSTM in [26] for U-1 and U-2, respectively. According to the figure, the proposed HyDNN model has a similar trend with [45] and provides better performance as compared to other models for U-2 in terms of SER. In the case of U-1, the proposed method outperforms the existing models by 10dB SNR gain. The SER versus SNR graphs demonstrate that the performance of the proposed HyDNN network with the other existing approaches is relatively higher for U-1 with the ranges of lower SNR values.

Figure 13 shows the comparison of the proposed system results regarding SER achievement and different SNR values with different system configurations. The simulation results are taken with a learning rate of 0.01 during the model training. To justify of ICI and ISI handling capability of the proposed model, different CP values and pilot numbers are considered for system configuration. From Fig. 13, it is indicated that with the CP=20, pilot=64 and CP=20, pilot=32, the proposed model showed almost the same SER performance with SNRs for the U-1 and U-2, respectively. In addition, with a fixed pilot of 64 and changing the CP to 16, the proposed model performance is not much different. Furthermore, with the value of CP=16 and pilot=32, the proposed model showed a little bit less performance than other configurations for both Us.

B. COMPLEXITY ANALYSIS

In this section, the proposed model complexity is explained. By taking into account the quantity of floating-point operations, computational complexity is quantified in terms of time. The complexity of the 1-D CNN model can be described

TABLE 3. Online computational time (in seconds) and FLOPs for the different estimation methods.

Methods	Online Estimation Time	Offline Training Time	FLOPs Number
LS+MMSE	33.30907	-	4.5×10^8
ML	3.60645	-	9.4×10^6
HyDNN	For LR=0.01, R_T=9.85619; For LR=0.001, R_T=9.91830	For LR=0.01, R_T=18214.45; For LR=0.001, R_T=29274.60	7.9×10^8

R_T=Computational time; LR=Learning rate;

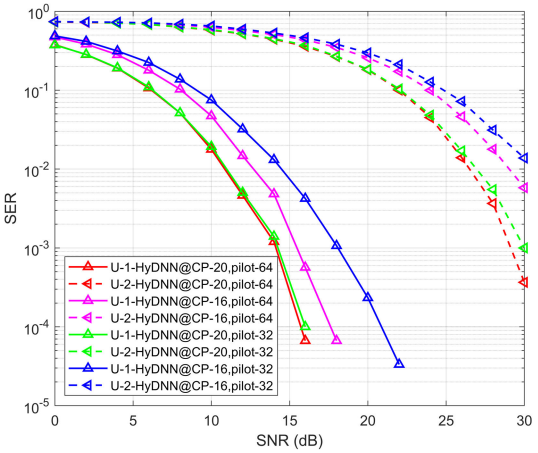

FIGURE 13. Comparison of the proposed system results regarding SER achievement and different SNR values with different system configurations.

as: $\mathcal{O}(N, K)$ [24] where N stands for the number of the filters and K for the convolutional kernel. The complexity of the LSTM is given by: $\mathcal{O}(L)$ [29] where L is the weight size of hidden layers. So, Consequently, the complexity of the BiLSTM model can be written as $\mathcal{O}(2L)$ as it flows in a bi-directional mode. However, the HyDNN detection model complexity can be represented as: $\mathcal{O}(N, K + 2L)$. In the traditional LS and MMSE-SIC detection method, the complexity is as: $\mathcal{O}(4M + 2)$, where M stands for the modulation order. The complexity of the ML approach is further represented as follows: $\mathcal{O}(2M)$. The above complexity of the HyDNN model is involved in the offline training process which required a long running time during the training of the model. However, the proposed HyDNN model includes many parameters, the complexity can be decreased by using parallelization of the graphics processing unit (GPU) [46] in the actual online process. Table 3 shows the justification of each method's result of the online process which is executed by proposed algorithms. In addition, floating point operations (FLOPs) are also presented in the table. Although the proposed model required higher complexity than others, its estimation performance is higher than all and the computational time can be reduced by using GPU parallel computing.

V. CONCLUSION

A multiuser CE and SD method in uplink transmission for the NOMA-OFDM is presented in this study using a HyDNN network. The HyDNN model is constructed by a 1D-CNN and a BiLSTM model. The proposed HyDNN model works better than the traditional SIC-based techniques in terms of symbol recovery rate. It is demonstrated that the proposed HyDNN network is more efficient for radio resources like the strength of signals, pilot symbols, and CP data than traditional CE approaches like MMSE, LS, and ML. Additionally, the proposed model outperforms the CNN and BiLSTM models when using the same channel parameters. The proposed model shows high learning ability even though the model with training less learning rate. Additionally, the proposed system SER detection performance rate is significantly higher than that of existing approaches. Future applications of this technique include more intricate systems like the NOMA system with MIMO communication. It can also be used in physical layers applications like reconfigurable reflecting surfaces-based wireless networks.

REFERENCES

[1] X. Chen, G. Liu, Z. Ma, Zhang, Xi, W. Xu, and P. Fan, "Optimal power allocations for non-orthogonal multiple access over 5G full/half-duplex relaying mobile wireless networks," *IEEE Trans. Wireless Commun.*, vol. 18, no. 1, pp. 77–92, Jan. 2019.

[2] Y. Saito, Y. Kishiyama, A. Benjebbour, T. Nakamura, A. Li, and K. Higuchi, "Non-orthogonal multiple access (NOMA) for cellular future radio access," in *Proc. IEEE 77th Veh. Technol. Conf. (VTC Spring)*, Jun. 2013, pp. 1–5.

[3] Y.-R. Lee, W.-S. Lee, J.-S. Jung, C.-Y. Park, Y.-H. You, and H.-K. Song, "Hybrid beamforming with reduced RF chain based on PZF and PD-NOMA in mmWave massive MIMO systems," *IEEE Access*, vol. 9, pp. 60695–60703, 2021.

[4] D. Hwang, J. Yang, S. S. Nam, and H.-K. Song, "Optimal multi-antenna transmission for the cooperative non-orthogonal multiple-access system," *Appl. Sci.*, vol. 11, no. 5, p. 2203, Mar. 2021.

[5] X. Wang, P. Zhu, D. Li, Y. Xu, and X. You, "Pilot-assisted SIMO-NOMA signal detection with learnable successive interference cancellation," *IEEE Commun. Lett.*, vol. 25, no. 7, pp. 2385–2389, Jul. 2021.

[6] K. Higuchi and A. Benjebbour, "Non-orthogonal multiple access (NOMA) with successive interference cancellation for future radio access," *IEICE Trans. Commun.*, vol. E98.B, no. 3, pp. 403–414, 2015.

[7] V. Andiappan and V. Ponnusamy, "Deep learning enhanced NOMA system: A survey on future scope and challenges," *Wireless Pers. Commun.*, vol. 123, no. 1, pp. 839–877, Mar. 2022.

[8] C. Chun, J. Kang, and I. Kim, "Deep learning-based channel estimation for massive MIMO systems," *IEEE Wireless Commun. Lett.*, vol. 8, no. 4, pp. 1228–1231, Aug. 2019.

[9] H. Hua, X. Wang, and Y. Xu, "Signal detection in uplink pilot-assisted multi-user MIMO systems with deep learning," in *Proc. Comput., Commun. IoT Appl. (ComComAp)*, Oct. 2019, pp. 369–373.

[10] X. Miao, D. Guo, and X. Li, "Grant-free NOMA with device activity learning using long short-term memory," *IEEE Wireless Commun. Lett.*, vol. 9, no. 7, pp. 981–984, Jul. 2020.

[11] T. O'Shea and J. Hoydis, "An introduction to deep learning for the physical layer," *IEEE Trans. Cognit. Commun. Netw.*, vol. 3, no. 4, pp. 563–575, Dec. 2017.

[12] T. Zhao, F. Li, and P. Tian, "A deep-learning method for device activity detection in mMTC under imperfect CSI based on variational-autoencoder," *IEEE Trans. Veh. Technol.*, vol. 69, no. 7, pp. 7981–7986, Jul. 2020.
[13] C. She, R. Dong, Z. Gu, Z. Hou, Y. Li, W. Hardjawana, C. Yang, L. Song, and B. Vucetic, "Deep learning for ultra-reliable and low-latency communications in 6G networks," *IEEE Netw.*, vol. 34, no. 5, pp. 219–225, Sep. 2020.
[14] M. S. Sim, Y. Lim, S. H. Park, L. Dai, and C. Chae, "Deep learning-based mmWave beam selection for 5G NR/6G with sub-6 GHz channel information: Algorithms and prototype validation," *IEEE Access*, vol. 8, pp. 51634–51646, 2020.
[15] Z. Mao, X. Liu, and M. Peng, "Channel estimation for intelligent reflecting surface assisted massive MIMO systems—A deep learning approach," *IEEE Commun. Lett.*, vol. 26, no. 4, pp. 798–802, Apr. 2022.
[16] I. A. Nemer, T. R. Sheltami, S. Belhaiza, and A. S. Mahmoud, "Energy-efficient UAV movement control for fair communication coverage: A deep reinforcement learning approach," *Sensors*, vol. 22, no. 5, p. 1919, Mar. 2022.
[17] J. An, C. Xu, Q. Wu, D. W. K. Ng, M. D. Renzo, C. Yuen, and L. Hanzo, "Codebook-based solutions for reconfigurable intelligent surfaces and their open challenges," *IEEE Wireless Commun.*, early access, Nov. 15, 2022, doi: 10.1109/MWC.010.2200312.
[18] M. AbdelMoniem, S. M. Gasser, M. S. El-Mahallawy, M. W. Fakhr, and A. Soliman, "Enhanced NOMA system using adaptive coding and modulation based on LSTM neural network channel estimation," *Appl. Sci.*, vol. 9, no. 15, p. 3022, Jul. 2019.
[19] Y. Lu, P. Cheng, Z. Chen, W. H. Mow, Y. Li, and B. Vucetic, "Deep multi-task learning for cooperative NOMA: System design and principles," *IEEE J. Sel. Areas Commun.*, vol. 39, no. 1, pp. 61–78, Jan. 2021.
[20] A. Emir, F. Kara, H. Kaya, and H. Yanikomeroglu, "Deep learning empowered semi-blind joint detection in cooperative NOMA," *IEEE Access*, vol. 9, pp. 61832–61852, 2021.
[21] H. Ye, G. Y. Li, and B. Juang, "Power of deep learning for channel estimation and signal detection in OFDM systems," *IEEE Wireless Commun. Lett.*, vol. 7, no. 1, pp. 114–117, Feb. 2018.
[22] C. Lin, Q. Chang, and X. Li, "A deep learning approach for MIMO-NOMA downlink signal detection," *Sensors*, vol. 19, no. 11, p. 2526, Jun. 2019.
[23] P. Dong, H. Zhang, G. Y. Li, I. S. Gaspar, and N. NaderiAlizadeh, "Deep CNN-based channel estimation for mmWave massive MIMO systems," *IEEE J. Sel. Topics Signal Process.*, vol. 13, no. 5, pp. 989–1000, Sep. 2019.
[24] S. Kiranyaz, O. Avci, O. Abdeljaber, T. Ince, M. Gabbouj, and D. J. Inman, "1D convolutional neural networks and applications: A survey," *Mech. Syst. Signal Process.*, vol. 151, Apr. 2021, Art. no. 107398.
[25] L. Chuan, C. Qing, and L. Xianxu, "Uplink NOMA signal transmission with convolutional neural networks approach," *J. Syst. Eng. Electron.*, vol. 31, no. 5, pp. 890–898, Oct. 2020.
[26] Y. Xie, K. C. Teh, and A. C. Kot, "Deep learning-based joint detection for OFDM-NOMA scheme," *IEEE Commun. Lett.*, vol. 25, no. 8, pp. 2609–2613, Aug. 2021.
[27] Z. Yin, J. Chen, G. Li, H. Wang, W. He, and Y. Ni, "A deep learning-based user selection scheme for cooperative NOMA system with imperfect CSI," *Wireless Commun. Mobile Comput.*, vol. 2022, pp. 1–13, May 2022.
[28] D. Haviv, A. Rivkind, and O. Barak, "Understanding and controlling memory in recurrent neural networks," in *Proc. Int. Conf. Mach. Learn.*, Sep. 2019, pp. 2663–2671.
[29] S. Hochreiter and J. Schmidhuber, "Long short-term memory," *Neural Comput.*, vol. 9, no. 8, pp. 1735–1780, Nov. 1997.
[30] W. Xu, J. An, Y. Xu, C. Huang, L. Gan, and C. Yuen, "Time-varying channel prediction for RIS-assisted MU-MISO networks via deep learning," *IEEE Trans. Cognit. Commun. Netw.*, vol. 8, no. 4, pp. 1802–1815, Dec. 2022.
[31] S. Pandya, M. A. Wakchaure, R. Shankar, and J. R. Annam, "Analysis of NOMA-OFDM 5G wireless system using deep neural network," *J. Defense Model. Simul., Appl., Methodol., Technol.*, vol. 19, no. 4, pp. 799–806, Oct. 2022.
[32] D. Tian, P. Miao, H. Peng, W. Yin, and X. Li, "Volterra-aided neural network equalization for channel impairment compensation in visible light communication system," *Photonics*, vol. 9, no. 11, p. 845, Nov. 2022.
[33] M. H. Rahman, M. A. S. Sejan, M. A. Aziz, J. Baik, D. Kim, and H. Song, "Deep learning based improved cascaded channel estimation and signal detection for reconfigurable intelligent surfaces-assisted MU-MISO systems," *IEEE Trans. Green Commun. Netw.*, early access, Jan. 17, 2023, doi: 10.1109/TGCN.2023.3237132.
[34] R. L. Abduljabbar, H. Dia, and P.-W. Tsai, "Unidirectional and bidirectional LSTM models for short-term traffic prediction," *J. Adv. Transp.*, vol. 2021, pp. 1–16, Mar. 2021.
[35] S. Siami-Namini, N. Tavakoli, and A. S. Namin, "The performance of LSTM and BiLSTM in forecasting time series," in *Proc. IEEE Int. Conf. Big Data (Big Data)*, Dec. 2019, pp. 3285–3292.
[36] M. H. Rahman, M. A. S. Sejan, S.-G. Yoo, M.-A. Kim, Y.-H. You, and H.-K. Song, "Multi-user joint detection using bi-directional deep neural network framework in NOMA-OFDM system," *Sensors*, vol. 22, no. 18, p. 6994, Sep. 2022.
[37] A. L. Ha, T. Van Chien, T. H. Nguyen, W. Choi, and V. D. Nguyen, "Deep learning-aided 5G channel estimation," in *Proc. 15th Int. Conf. Ubiquitous Inf. Manage. Commun. (IMCOM)*, Jan. 2021, pp. 1–7.
[38] Q. Bai, J. Wang, Y. Zhang, and J. Song, "Deep learning-based channel estimation algorithm over time selective fading channels," *IEEE Trans. Cognit. Commun. Netw.*, vol. 6, no. 1, pp. 125–134, Mar. 2020.
[39] P. Chen and H. Kobayashi, "Maximum likelihood channel estimation and signal detection for OFDM systems," in *Proc. IEEE Int. Conf. Communications. Conf. (ICC)*, Aug. 2002, pp. 1640–1645.
[40] M.-H. Hsieh and C.-H. Wei, "Channel estimation for OFDM systems based on comb-type pilot arrangement in frequency selective fading channels," *IEEE Trans. Consum. Electron.*, vol. 44, no. 1, pp. 217–225, Feb. 1998.
[41] L. Shi, B. Guo, and L. Zhao, "Block-type pilot channel estimation for OFDM systems under frequency selective fading channels," in *Proc. IET Int. Commun. Conf. Wireless Mobile Comput. (CCWMC)*, Shanghai, China, Dec. 2009, pp. 21–24.
[42] S. Khan, S. Durrani, M. B. Shahab, S. J. Johnson, and S. Camtepe, "Joint user and data detection in grant-free NOMA with attention-based BiLSTM network," 2022, *arXiv:2209.06392*.
[43] T. van Laarhoven, "L2 regularization versus batch and weight normalization," 2017, *arXiv:1706.05350*.
[44] D. P. Kingma and J. Ba, "Adam: A method for stochastic optimization," 2014, *arXiv:1412.6980*.
[45] A. Kumar and K. Kumar, "Deep learning-based joint NOMA signal detection and power allocation in cognitive radio networks," *IEEE Trans. Cognit. Commun. Netw.*, vol. 8, no. 4, pp. 1743–1752, Dec. 2022.
[46] I. Goodfellow, Y. Bengio, and A. Courville, *Deep Learning*. Cambridge, MA, USA: MIT Press, Nov. 2016.

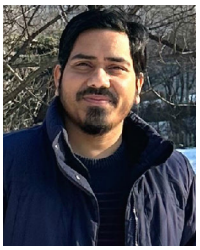

MD HABIBUR RAHMAN received the B.S. degree in electrical and electronic engineering from Islamic University, Kushtia, Bangladesh, in 2014, and the M.S. degree in electronic engineering from Pukyong National University, Busan, Republic of Korea, in August 2020. He is currently pursuing the Ph.D. degree with the Department of Information and Communication Engineering and the Department of Convergence Engineering for Intelligent Drone, Sejong University, Seoul, Republic of Korea. His current research interests include wireless sensor networks, machine learning, wireless communication, intelligent reflective surfaces, visible light communication, and the IoT applications.

MOHAMMAD ABRAR SHAKIL SEJAN received the B.S. and M.S. degrees in computer science and engineering from Islamic University, Kushtia, Bangladesh, in 2014 and 2016, respectively, and the Ph.D. degree in electronic engineering from Pukyong National University, Busan, Republic of Korea, in February 2022. Currently, he is a Research Professor with the Information and Communication Engineering Department and the Department of Convergence Engineering for Intelligent Drone, Sejong University, Seoul, Republic of Korea. His current research interests include visible light communication, optical communication, wireless sensor networks, reconfigurable intelligent surface, protocol design for communication, and modulation techniques in VLC and IoT applications. He serves as a reviewer for different journals and international conferences.

MD ABDUL AZIZ received the B.S. and M.S. degrees in electrical and electronic engineering from Islamic University, Kushtia, Bangladesh, in 2014 and 2018, respectively. He is currently pursuing the Ph.D. degree with the Department of Information and Communication Engineering and the Department of Convergence Engineering for Intelligent Drone, Sejong University, Seoul, Republic of Korea. His current research interests include machine learning, wireless communication, and intelligent reflective surfaces.

YOUNG-HWAN YOU received the B.S., M.S., and Ph.D. degrees in electronic engineering from Yonsei University, Seoul, South Korea, in 1993, 1995, and 1999, respectively. From 1999 to 2002, he was a Senior Researcher with the Wireless PAN Technology Project Office, Korea Electronics Technology Institute, Seongnam, South Korea. Since 2002, he has been a Professor with the Department of Computer Engineering and the Department of Convergence Engineering for Intelligent Drone, Sejong University, Seoul. His current research interests include wireless communications and signal processing, with a particular focus on 4G LTE, the NB-IoT, 5G new radio, and ultrareliable low-latency communication.

HYOUNG-KYU SONG received the B.S., M.S., and Ph.D. degrees in electronic engineering from Yonsei University, Seoul, South Korea, in 1990, 1992, and 1996, respectively. From 1996 to 2000, he was a Managerial Engineer with the Korea Electronics Technology Institute (KETI), South Korea. Since 2000, he has been a Professor with the Department of Information and Communication Engineering and the Department of Convergence Engineering for Intelligent Drone, Sejong University, Seoul. His current research interests include digital and data communications, information theory, and their applications, with an emphasis on mobile communications.